Hindawi Publishing Corporation
Journal of Spectroscopy
Volume 2014, Article ID 751458, 9 pages
http://dx.doi.org/10.1155/2014/751458

Research Article

Effects of UV-B Radiation on Near-Infrared Spectroscopy and Identification of *Puccinia striiformis* f. sp. *tritici*

Pei Cheng,[1] Xiaolong Li,[1] Feng Qin,[1] Longlian Zhao,[2] Junhui Li,[2] Zhanhong Ma,[1] and Haiguang Wang[1]

[1]*College of Agriculture and Biotechnology, China Agricultural University, Beijing 100193, China*
[2]*College of Information and Electrical Engineering, China Agricultural University, Beijing 100083, China*

Correspondence should be addressed to Haiguang Wang; wanghaiguang@cau.edu.cn

Received 12 November 2014; Accepted 10 December 2014; Published 29 December 2014

Academic Editor: Austin Nevin

Based on near-infrared spectra of three physiological races of *Puccinia striiformis* f. sp. *tritici* (i.e., CYR31, CYR32, and CYR33) irradiated under four UV-B intensities (i.e., 0, 150, 200, and 250 μw/cm^2), the effects of UV-B radiation on near-infrared spectroscopy of the pathogen were investigated in spectral region 4000–10000 cm^{-1}, and support vector machine models were built to identify UV-B radiation intensities and physiological races, respectively. The results showed that the spectral curves under UV-B radiation treatments exhibited great differences compared with the corresponding control treatment (0 μw/cm^2) in the spectral regions 5300–5600 cm^{-1} and 7000–7400 cm^{-1} and that the absorbance values of all the three physiological races increased with the enhancement of UV-B radiation intensity. Based on near-infrared spectroscopy, different UV-B radiation intensities could be identified and different physiological races could be distinguished from each other with high accuracies. The results demonstrated the utility and stability of the proposed method to identify the physiological races.

1. Introduction

Wheat stripe rust caused by *Puccinia striiformis* f. sp. *tritici* (*Pst*) is an important fungal disease. In China, this disease affects wheat production in various degrees every year. Usually, yield loss caused by this disease ranges from 10% to 30%. If serious outbreak of the disease occurs, severe yield loss up to 50% and even 100% may be caused [1]. Wheat stripe rust is a typical air-borne disease and it mainly relies on urediospores' long-distance spread to accomplish disease cycles. But *Pst* urediospores are sensitive to ultraviolet (UV) radiation, moisture, temperature, and other external environmental conditions [1]. Therefore, the environmental changes can largely affect the occurrence and development of wheat stripe rust [1]. Due to human activities, the exacerbated atmospheric ozone depletion results in an increase of UV radiation reaching the earth's surface, and then the enhanced UV radiation can affect plant pathogens, host plants, and plant diseases [2]. Currently, UV radiation has been regarded as an important environmental factor that can affect development and epidemics of plant diseases [3, 4]. Therefore, strengthening research on the effects of UV radiation on plant pathogens and plant diseases is critical to sustainable control of plant diseases and food security.

In the background of global climate change, widespread attention has been attracted to the effects of UV radiation on crops and plant pathogens. The studies on effects of UV radiation on physiology, biochemistry, growth, and development of plants showed that UV radiation can have impacts on crop photosynthesis [5–7], regulation of secondary metabolites [8, 9], morphological construction [10], and so forth. UV radiation can affect spore germination, germ tube elongation, mycelial growth, and pathogen survival [3, 11–14]. Several studies on the effects of UV radiation on wheat stripe rust and the causal agent have been conducted. Jing et al. [15] reported that UV radiation could change the pathogenicity of *Pst*, extend latent period of wheat stripe rust, reduce infection type, length of uredinium, sporulation quantity, and disease severity, and shorten sporulation period. Seven virulence mutant strains were obtained from *Pst* spores that were exposed to UV radiation [16]. UV radiation could cause some changes in genomic DNA of *Pst* and there

were significant differences of DNA polymorphisms between wild-type *Pst* strains and virulence mutant strains obtained after UV irradiation [17, 18]. The above studies showed that UV radiation could have influence on *Pst* and could cause some changes of *Pst* characteristics. In the previous study, near-infrared spectroscopy (NIRS) was applied to identify wheat stripe rust pathogen and wheat leaf rust pathogen (*P. recondita* f. sp. *tritici*), and high identification accuracy was obtained [19]. However, as an external environmental factor, whether UV radiation can affect the near-infrared (NIR) spectral characteristics of *Pst* and whether it can further affect identification of *Pst* are not yet known. Therefore, to detect biology indicators of wheat stripe rust pathogen and to identify the physiological races of *Pst*, it is urgently needed to carry out the studies on the effects of UV radiation on NIR spectroscopy and identification performance of *Pst*. Thus, this will provide the basis and support for pathogen monitoring and epidemic prediction of wheat stripe rust.

As a nonpolluting and nondestructive technology, NIRS can be implemented to both quantitative analysis and qualitative analysis of the samples quickly and accurately, and now it has been widely used in food, chemicals, pharmaceuticals, agriculture, petroleum industry, and other related fields [20–22]. In recent years, the studies on the detection of plant diseases based on NIRS technology increased gradually. Feng et al. [23] realized rapid and early nondestructive detection of soybean pod anthracnose using visible/near-infrared spectroscopy technology combined with successive projections algorithm (SPA) and least square support vector machine (LS-SVM). Chen et al. [24] estimated disease severity of verticillium wilt on cotton leaves using visible/near-infrared spectroscopy and all multiple inversion models built for estimation of disease severity reached the best significant level. Wu et al. [25] constructed a backpropagation (BP) model for the early detection of gray mold on eggplant leaves using visible/near-infrared spectroscopy technology and the correct rate was 88%. Using NIRS technology combined with discriminant partial least squares (DPLS), Li et al. [26] developed a method to discriminate wheat stripe rust and wheat leaf rust, and the early diagnosis of these two major diseases on wheat could be achieved using the method. However, there are still no reports about the effects of UV radiation on NIR spectroscopy and identification of *Pst*.

In this study, three current predominant races (i.e., CYR31, CYR32, and CYR33) of wheat stripe rust pathogen were irradiated under different UV-B intensities (i.e., 0, 150, 200, and 250 μw/cm^2) and the effects of UV-B radiation on NIR spectroscopy and identification of *Pst* were investigated. UV-B intensity identification models and *Pst* race identification models after UV-B irradiation were built using NIRS technology combined with support vector machine (SVM).

2. Materials

Three predominant physiological races including CYR31, CYR32, and CYR33 in China were used in this study. Mingxian 169, a wheat cultivar which is susceptible to all known physiological races of *Pst*, was selected as the host cultivar to multiply wheat stripe rust pathogen. The races were multiplied in the artificial climate chamber in the Lab of Plant Disease Epidemiology, Department of Plant Pathology, China Agricultural University.

Wheat was planted as follows: firstly, the seeds of Mingxian 169 were soaked for 24 h in sterile water and were then sowed in pots (10 cm in diameter) with about 20 seeds per pot; subsequently, the pots were incubated in the artificial climate chamber at 11–13°C and 60–70% relative humidity (RH) with 12 h light per day (10000 lux).

As the first leaves of wheat seedlings fully expanded, artificial spray inoculation of *Pst* was conducted. Pathogen spores stored in the liquid nitrogen container were taken out and were reactivated in warm water of 40°C for 5 min and were then hydrated at 4°C for 12 h. To improve inoculation efficiency, wax on leaf surface was removed by rubbing the surface using fingers dipped with sterile water before inoculation. Spore suspension was made with 0.2% Tween 80 and then was sprayed on the leaves of wheat seedlings using a small sprinkling can. Wheat seedlings were immediately placed into a moist chamber in dark conditions at 11–13°C for 24 h. Then the inoculated wheat seedlings were incubated in the artificial climate chamber under the conditions described above. After 15 days, uredinia started to appear on the leaves of the inoculated seedlings. To ensure that there were adequate pathogen spores for further experiments, 110 pots of wheat seedlings were used to multiply the spores of each physiological race, respectively. To reduce experimental error caused by multiple collections, enough spores of each race were collected only one time during the peak period of disease progress and then were reserved in three different glass tubes in a dryer at 4°C for following experiments.

3. Methods

3.1. UV-B Radiation of Wheat Stripe Rust Pathogen. UV-B radiation was provided by three 30 W UV-B lamps (wavelength range: 290–320 nm; the maximum emission wavelength: 313 nm) (Beijing Lighting Research Institute, Beijing, China) that were mounted in a sealed box. Different UV-B radiation intensities were obtained by adjusting the distance between the lamps and the experimental materials. UV-B radiation was measured using a UV-B 297 radiation meter (the wavelength range it can measure: 275–330 nm; the peak wavelength it can measure: 297 nm; sensitivity: 0.1 μw/cm^2) (Beijing Normal University Photoelectric Instrument Factory, Beijing, China). In this study, the three current predominant physiological races of *Pst* were irradiated for 60 min under four different UV-B radiation intensities (i.e., 0, 150, 200, and 250 μw/cm^2), respectively. And then NIR spectra of the irradiated spores of each physiological race were collected. To obtain the UV-B intensities (150, 200, and 250 μw/cm^2), the distances between the UV-B lamps and the pathogen spores were 14, 10.5, and 7 cm, respectively.

3.2. Acquisition of Near-Infrared Spectra. After the three current predominant races of *Pst* were irradiated under different UV-B intensities, the acquisition of NIR spectra

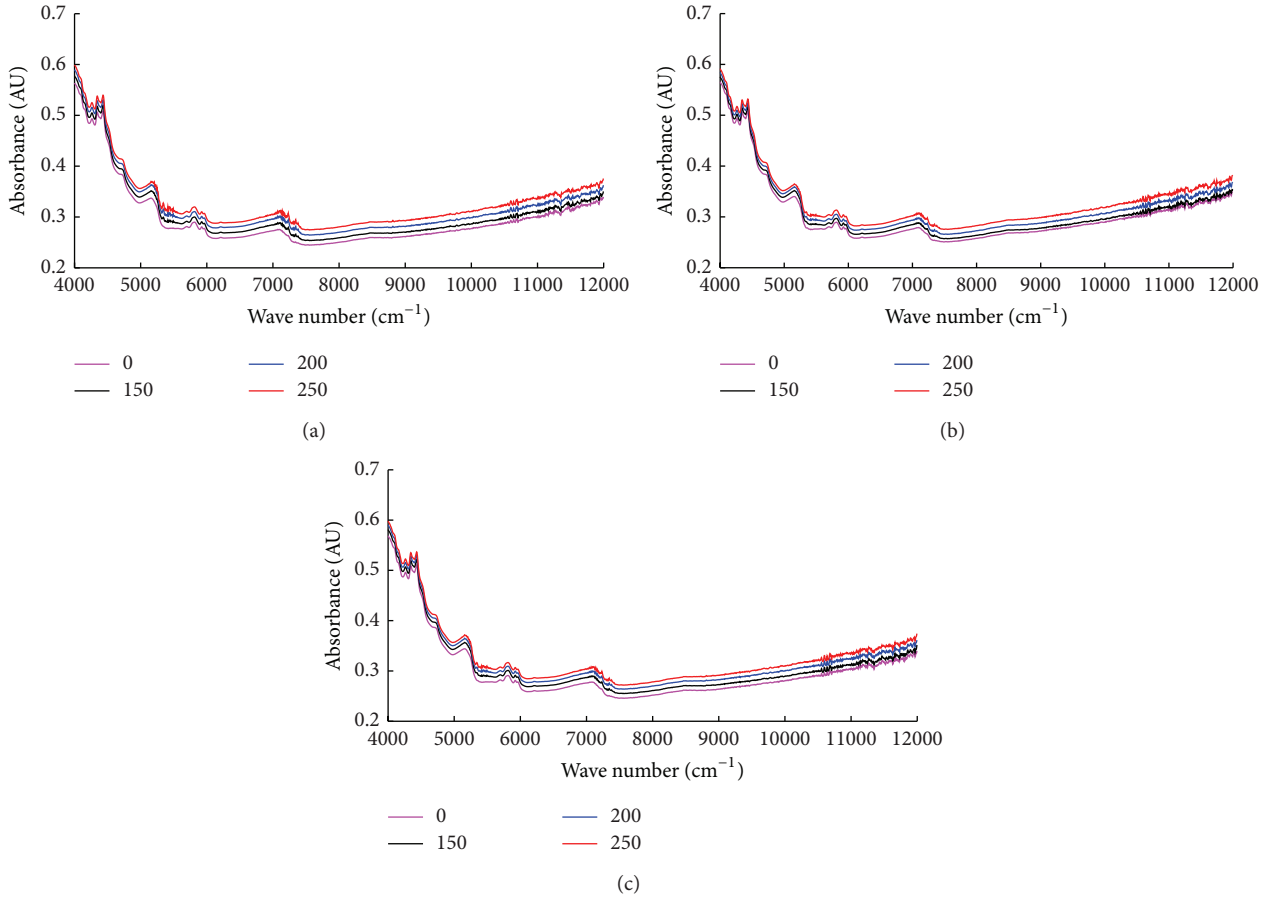

Figure 1: Spectral curves for each physiological race of wheat stripe rust pathogen which was irradiated under different UV-B intensities. (a) was for CYR31, (b) was for CYR32, and (c) was for CYR33. The unit of UV-B intensity is μw/cm^2.

of *Pst* was performed by using FT-NIR MPA spectrometer (Bruker, Germany). While NIR spectra were collected, 30 samples of each physiological race were set for each UV-B radiation treatment. So 120 spectra under four different UV-B radiation intensities were collected for each physiological race, and thus a total of 360 spectra were obtained. Integrating sphere diffuse reflectance method was used to collect the spectra of *Pst*. The measured spectral range was 4000–12000 cm^{-1}, the spectral resolution was set as 8 cm^{-1}, and the number of scan processes was 32. Before scanning, 40 mg wheat stripe rust urediospores were placed into a sample cup (4 mm in diameter). The tightness of the spore samples in the cup should be kept in the same consistency in order to reduce the experimental error caused by different tightness. For each physiological race, averaging the 30 spectra of each UV-B radiation treatment was conducted and then four spectra were obtained as shown in Figure 1. Similarly, for each UV-B radiation treatment, averaging 30 spectra of each physiological race was conducted and three spectra were then obtained as shown in Figure 2. In Figures 1 and 2, some level of noise can be observed from the spectra. To reduce the disturbance of the noise, the spectra in 4000–10000 cm^{-1} were used to establish the UV-B intensity identification models and *Pst* physiological race identification models.

3.3. Establishment of UV-B Intensity Identification Models and Pst Physiological Race Identification Models. Support vector machine with good generalization ability is a pattern recognition method based on VC dimension theory and structural risk minimization principle [27]. In this study, SVM models for UV-B radiation intensity identification and *Pst* race identification were established by using LIBSVM package developed by Chih-Jen Lin Group from Taiwan [28]. Totally, four UV-B intensity identification models and five race identification models were established in this study. To establish intensity identification models, for individual race, 20 spectra were randomly selected from 30 spectra of each UV-B intensity treatment to set up training set including 80 spectra, and the rest were treated as testing set including 40 spectra; for mixed physiological races with the three races, the training set was formed of 240 spectra randomly selected from UV-B radiation treatments (60 spectra per treatment) and the remaining 120 spectra were treated as the testing set. To establish race identification models, for individual UV-B intensity, 20 spectra were randomly selected from 30 spectra of each race to set up training set including 60 spectra, and the rest were treated as testing set including 30 spectra; for mixed treatment of four UV-B radiation intensities, the training set was formed of 240 spectra randomly selected from the spectra

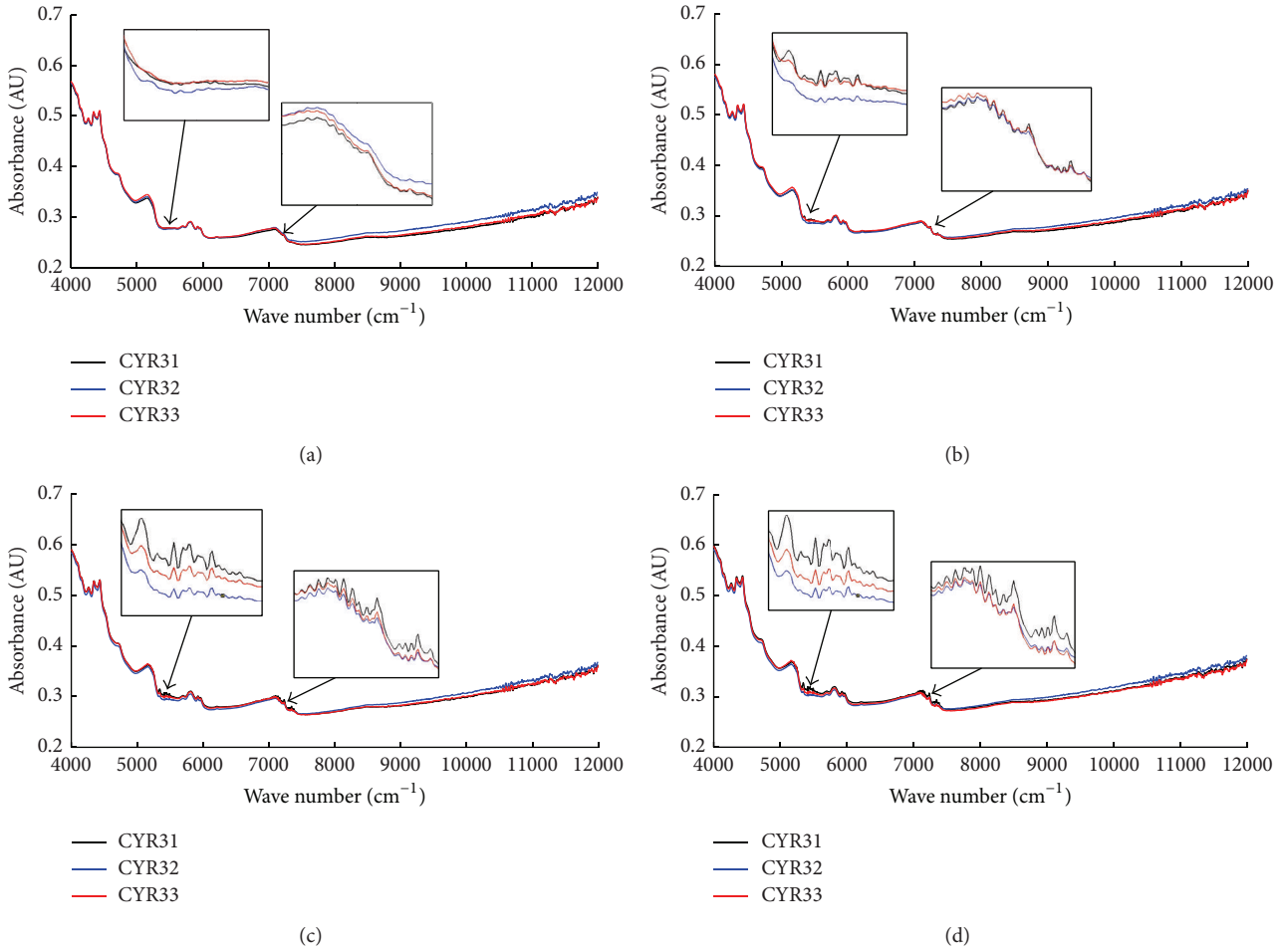

Figure 2: Spectral curves of the three physiological races of wheat stripe rust pathogen under each UV-B intensity exposure. (a) UV-B intensity was 0 μw/cm^2, (b) UV-B intensity was 150 μw/cm^2, (c) UV-B intensity was 200 μw/cm^2, and (d) UV-B intensity was 250 μw/cm^2. The spectral ranges of enlarged section in the diagram were 5300–5600 cm^{-1} and 7000–7400 cm^{-1}, respectively.

of different races (80 spectra per race) and the remaining 120 spectra were treated as the testing set. In the spectral region 4000–10000 cm^{-1}, radial basis function (RBF) that can preferably process complex nonlinear data was used as the kernel function of SVM to establish identification models. Using grid search algorithm, both the optimal penalty parameter C and the optimal kernel function parameter γ were searched in the searching range 2^{-10}–2^{10} with the searching step equal to 1 for each model. Classification accuracies were computed at all points within the grid and the values of C and γ were selected as the optimal parameters as the classification accuracy of the training set was the highest. Then the identification models were used to identify UV-B radiation intensities and *Pst* physiological races, respectively.

4. Results

4.1. Changes of NIR Spectra of Pst after UV-B Irradiation. As shown in Figure 1, for the same physiological race of *Pst*, the NIR spectral characteristics were largely influenced by UV-B radiation. The absorbance values of the same physiological race of *Pst* increased with the increase of the UV-B radiation intensity. As shown in Figure 2(a), the differences between the spectra of the three physiological races without UV-B irradiation (UV-B intensity = 0 μw/cm^2) were relatively small and the differences may result from the differences between physiological races of *Pst*. Figures 2(b), 2(c), and 2(d) showed that there were great differences within spectral ranges 5300–5600 cm^{-1} and 7000–7400 cm^{-1} between the spectra of the three physiological races after UV-B irradiation (UV-B intensity = 150, 200, and 250 μw/cm^2) and the corresponding spectra of the physiological races shown in Figure 2(a). And the differences increased with the enhancement of UV-B radiation intensity.

4.2. SVM-Based Identification Results of Different UV-B Intensity Treatments. For each physiological race of *Pst*, SVM models were established to identify different UV-B radiation intensities. The searching results of the parameters C and γ when the intensity identification accuracy was the highest were shown in Table 1 (Model 1, Model 2, and Model 3). For the SVM models established to identify different UV-B

Table 1: The best indexes for UV-B intensity identification SVM models.

Model number	Model name	Total number of samples for training set	Total number of samples for testing set	Optimal parameters		Overall identification accuracy of training set/%	Overall identification accuracy of testing set/%
				C	γ		
Model 1	UV-B intensity identification model for CYR31	80	40	$9.77E-04$	0.5	100.00	97.50
Model 2	UV-B intensity identification model for CYR32	80	40	$9.77E-04$	512	100.00	100.00
Model 3	UV-B intensity identification model for CYR33	80	40	1	1024	100.00	87.50
Model 4	UV-B intensity identification model for mixed physiological races	240	120	2	128	100.00	95.83

radiation intensities when the spectra of the three different physiological races were mixed together, the searching results of the parameters C and γ were shown in Table 1 (Model 4). For different physiological races (CYR31, CYR32, CYR33, and mixed physiological races with the three races), the identification results of different UV-B radiation intensities were shown in Table 2.

As shown in Table 1 (Model 1) and Table 2, for CYR31, when $C = 9.77E-04$ and $\gamma = 0.5$, the UV-B radiation intensities of 80 samples in the training set were all correctly identified and the overall identification accuracy was 100.00%; however, the overall identification accuracy of the testing set was 97.50% and there was one identification error when UV-B intensity was 0 μw/cm^2. As shown in Table 1 (Model 2) and Table 2, for CYR32, when $C = 9.77E-04$ and $\gamma = 512$, 80 samples in the training set and 40 samples in the testing set were all correctly identified, and the overall identification accuracy of the training set and that of the testing set were both 100.00%. As shown in Table 1 (Model 3) and Table 2, for CYR33, when $C = 1$ and $\gamma = 1024$, 80 samples in the training set were correctly identified and the corresponding overall identification accuracy was 100.00%; however, the overall identification accuracy of the testing set was 87.50% and there were two and three identification errors under the UV-B intensities of 150 and 200 μw/cm^2, respectively. As shown in Table 1 (Model 4) and Table 2, for the established SVM models with 240 spectra as the training set and 120 spectra as the testing set, when $C = 2$ and $\gamma = 128$, 240 samples of four UV-B radiation intensities in the training set were all correctly identified and the overall UV-B intensity identification accuracy was 100.00%; however, the overall UV-B intensity identification accuracy of the testing set was 95.83%, and there were four identification errors and one identification error under the UV-B intensities of 200 μw/cm^2 (for CYR33) and 250 μw/cm^2 (for CYR31), respectively. The results indicated that the NIR spectral characteristics were greatly affected by the UV-B irradiation after the three physiological races of *Pst* were irradiated under four different UV-B intensities and that different UV-B intensities could be identified by the established SVM models with satisfactory accuracies.

4.3. SVM-Based Identification Results of the Three Physiological Races of Pst. For each UV-B radiation intensity, SVM models were established to identify different physiological races of *Pst*. The searching results of the parameters C and γ when the race identification accuracies of the models were the highest were shown in Table 3 (Model 5, Model 6, Model 7, and Model 8). For the models based on mixed treatment of four UV-B radiation intensities, the searching results of the parameters C and γ were shown in Table 3 (Model 9). For different UV-B irradiation intensities (i.e., 0, 150, 200, and 250 μw/cm^2 and mixed treatment of four UV-B radiation intensities), the race identification results of *Pst* were shown in Table 4.

As shown in Table 3 (Model 5) and Table 4, for 0 μw/cm^2 treatment, when $C = 4$ and $\gamma = 8$, the samples of the three physiological races in the training set and the testing set were all correctly identified, so the overall race identification accuracy of the training set and that of the testing set were both 100.00%. Table 3 (Model 6, Model 7, and Model 8) and Table 4 showed that, using the established SVM models, the three physiological races of *Pst* irradiated by each UV-B intensity (150, 200, or 250 μw/cm^2) still could be identified with good accuracy. Using Model 6, when $C = 0.5$ and $\gamma = 1024$, for 150 μw/cm^2 treatment, 60 samples of the three physiological races in the training set were all correctly identified and the overall race identification accuracy of the training set was 100.00%; however, the overall race identification accuracy of the testing set was 93.33% and there were two identification errors for CYR32. Using Model 7, for 200 μw/cm^2 treatment, when $C = 0.5$ and $\gamma = 256$, the spectral samples of the three physiological races in both the training set and the testing set were all correctly identified, and the overall race identification accuracy of the training set and that of the testing set were both 100.00%. Using Model 8, for 250 μw/cm^2 treatment, when $C = 0.5$ and $\gamma = 64$, the

Table 2: The UV-B intensity identification results of SVM models for CYR31, CYR32, CYR33, and mixed physiological races with the three races, respectively.

Model number	Physiological race	Sample category	Training set		Testing set	
			Number of samples	Number of correct identification samples	Number of samples	Number of correct identification samples
Model 1	CYR31	0 μw/cm^2	20	20	10	9
		150 μw/cm^2	20	20	10	10
		200 μw/cm^2	20	20	10	10
		250 μw/cm^2	20	20	10	10
Model 2	CYR32	0 μw/cm^2	20	20	10	10
		150 μw/cm^2	20	20	10	10
		200 μw/cm^2	20	20	10	10
		250 μw/cm^2	20	20	10	10
Model 3	CYR33	0 μw/cm^2	20	19	10	10
		150 μw/cm^2	20	20	10	8
		200 μw/cm^2	20	19	10	7
		250 μw/cm^2	20	20	10	10
Model 4	Mixed physiological races with the three races	0 μw/cm^2	60	60	30	30
		150 μw/cm^2	60	60	30	30
		200 μw/cm^2	60	60	30	26
		250 μw/cm^2	60	60	30	29

Note: for Model 1, Model 2, or Model 3, the total number of samples used for the training set was 80 (20 × 4), and the total number of samples used for the testing set was 40 (10 × 4). For Model 4, the total number of samples used for the training set was 240 (60 × 4), and the total number of samples used for the testing set was 120 (30 × 4).

Table 3: The best indexes for *Pst* race identification SVM models.

Model number	Model name	Total number of samples for training set	Total number of samples for testing set	Optimal parameters		Overall identification accuracy of training set/%	Overall identification accuracy of testing set/%
				C	γ		
Model 5	Race identification model of *Pst* under 0 μw/cm^2 treatment	60	30	4	8	100.00	100.00
Model 6	Race identification model of *Pst* under 150 μw/cm^2 treatment	60	30	0.5	1024	100.00	93.33
Model 7	Race identification model of *Pst* under 200 μw/cm^2 treatment	60	30	0.5	256	100.00	100.00
Model 8	Race identification model of *Pst* under 250 μw/cm^2 treatment	60	30	0.5	64	100.00	90.00
Model 9	Race identification model of *Pst* based on the mixed treatment of four UV-B radiation intensities	240	120	4	128	100.00	100.00

overall race identification accuracy of the training set was 100.00% and 60 samples of three physiological races in the training set were all correctly identified; however, the overall race identification accuracy of the testing set was 90.00% and there were three identification errors for CYR31. As shown in Table 3 (Model 9) and Table 4, for the established race identification SVM models with 240 spectra as the training set and 120 spectra as the testing set, when $C = 4$ and $\gamma = 128$, both the overall race identification accuracy of the training set and that of the testing set were 100.00%.

Table 4: The race identification results using SVM models for 0 μw/cm^2 treatment, 150 μw/cm^2 treatment, 200 μw/cm^2 treatment, 250 μw/cm^2 treatment, and total intensity treatments, respectively.

Model number	UV-B intensity	Sample category	Training set		Testing set	
			Number of samples	Number of correct identification samples	Number of samples	Number of correct identification samples
Model 5	0 μw/cm^2	CYR31	20	20	10	10
		CYR32	20	20	10	10
		CYR33	20	20	10	10
Model 6	150 μw/cm^2	CYR31	20	20	10	10
		CYR32	20	20	10	8
		CYR33	20	20	10	10
Model 7	200 μw/cm^2	CYR31	20	20	10	10
		CYR32	20	20	10	10
		CYR33	20	20	10	10
Model 8	250 μw/cm^2	CYR31	20	20	10	7
		CYR32	20	20	10	10
		CYR33	20	20	10	10
Model 9	Mixed treatment of four UV-B intensities	CYR31	80	80	40	40
		CYR32	80	80	40	40
		CYR33	80	80	40	40

Note: for Model 5, Model 6, Model 7, or Model 8, the total number of samples used for the training set was 60 (20 × 3), and the total number of samples used for the testing set was 30 (10 × 3). For Model 9, the total number of samples used for the training set was 240 (80 × 3), and the total number of samples used for the testing set was 120 (40 × 3).

5. Conclusions and Discussion

Wheat stripe rust is a kind of typical air-borne disease and its occurrence and epidemics are highly sensitive to the changes of UV radiation, moisture, temperature, and other external environmental conditions [1]. In particular, the effects of UV-B radiation on wheat stripe rust have attracted widespread attention in recent years. The effects of UV radiation on many characteristics of *Pst* such as biological effects [15], virulence mutation [16], and the changes of DNA polymorphism [17, 18] have been reported. However, there are still no studies on the effects of UV radiation on the characteristics of NIR spectra of *Pst*. Therefore, it is of great significance to investigate the effects of UV radiation on NIR spectroscopy and identification of *Pst* for pathogen monitoring and epidemic trend assessment of wheat stripe rust.

In this study, three current predominant races of *Pst* in China were irradiated under four different UV-B intensities, and then NIR spectra of the pathogen were collected. The effects of UV-B radiation on NIR spectra of the pathogen were investigated, and UV-B intensity identification models and race identification models were established based on the NIR spectra of wheat stripe rust pathogen using NIRS technology combined with SVM. The obtained results indicated that UV-B radiation had effects on NIR spectral characteristics of the pathogen and that the absorbance values of each physiological race increased with UV-B radiation intensity enhanced. After UV-B irradiation under 150, 200, and 250 μw/cm^2 intensity, there were great differences among the spectra of the three physiological races within 5300–5600 cm^{-1} and 7000–7400 cm^{-1} compared with the corresponding spectra of the races without UV-B radiation (UV-B intensity = 0 μw/cm^2), and the differences increased with UV-B irradiation intensity enhanced. For the three physiological races of *Pst* irradiated under four different UV-B intensities, the UV-B intensity identification accuracies of the training sets were all 100.00% and those of the testing sets were 97.50%, 100.00%, and 87.50%, respectively. UV-B radiation had great influence on NIR spectral characteristics of *Pst*, and thus different UV-B intensities could be identified according to the changes of spectral characteristics of *Pst* caused by different UV-B intensity radiation. When UV-B intensity was 0 μw/cm^2, the race identification accuracy of the training set and that of the testing set were both 100.00% for the race identification SVM models of the three physiological races. When UV-B intensities were 150, 200, and 250 μw/cm^2, for the race identification SVM models of the three physiological races, the race identification accuracies of the training sets were all 100.00% and those of the testing sets were 93.33%, 100.00%, and 90.00%, respectively. After irradiation under different UV-B intensities, NIR spectral characteristics of the three physiological races changed largely, but the three physiological races of *Pst* still could be accurately identified by using the race identification SVM models. This may be caused by the following two reasons. Firstly, the effects of

UV-B radiation on the NIR spectral characteristics were not enough to influence the identification performance of *Pst* physiological races and the race identification SVM models could distinguish the three physiological races of *Pst* according to the differences among themselves. Secondly, the effects of UV-B radiation on the NIR spectral characteristics were obvious to influence the identification performance of *Pst* physiological races. For the second reason, the effects may result from the changes of the nongenetic materials which reached the degree to distinguish the physiological races. The effects may also result from the changes of genetic materials and finally result in the appearance of new physiological races. Thus, the identification SVM models still could distinguish the three physiological races of *Pst*. However, no matter which inference is true, the above results indicated that the identification of wheat stripe rust based on NIRS was stable in a certain degree under UV-B radiation.

For plant pathologists working on wheat stripe rust, rapid and accurate identification of *Pst* physiological races is a very critical issue. Traditionally, identification of physiological races of plant pathogens depends on the responses of differential hosts to the races [1]. This traditional method is time-consuming and labor intensive. This study provided a fast method for identification of physiological races of *Pst* and also provided a reference for identification of physiological races of other fungi.

When the spores of wheat stripe rust pathogen were irradiated under different UV-B intensities, different UV-B intensities could be identified based on the changes of NIR spectral characteristics, and different physiological races also could be distinguished using NIRS technology. The results demonstrated the stability of *Pst* identification using NIRS technologies and showed the potential of NIRS to identify physiological races of fungi instead of the method using observation of different host responses. However, the results were obtained from laboratory experiments. For practical applications of these models, more samples of more physiological races and more samples collected from different regions are needed for further optimization of the models.

After UV irradiation, mutation of wheat stripe rust pathogen may occur. However, the mutation probability is very low and it ranges from 10^{-6} to 10^{-4} [16]. So this phenomenon may not affect the identification performance of physiological races of *Pst*. UV-B radiation dose ranges used in this study may not cause the changes of genetic materials. But once UV-B radiation dose is over the dose range that *Pst* can tolerate, the changes of genetic materials may be caused and thus pathogen mutation may be caused. Finally, new races or new pathogenic types may appear. Therefore, in further studies, screening mutant strains via increasing the UV-B radiation dose could be conducted, and then the changes of the NIR spectral characteristics of mutant strains and whether the mutant strains could be distinguished from wild strains based on NIRS could be investigated.

Conflict of Interests

The authors declare that there is no conflict of interests regarding the publication of this paper.

Authors' Contribution

Pei Cheng and Xiaolong Li contributed equally to this paper.

Acknowledgments

This study was supported by National Key Basic Research Program of China (2013CB127700), National Natural Science Foundation of China (31101393), and International Research Exchange Scheme of the Marie Curie Program of the 7th Framework Program (Ref. PIRSES-GA-2013-612659).

References

[1] Z. Q. Li and S. M. Zeng, *Wheat Rust in China*, China Agriculture Press, Beijing, China, 2002.

[2] W. J. Manning and A. V. Tiedemann, "Climate change: potential effects of increased atmospheric carbon dioxide (CO_2), ozone (O_3), and ultraviolet-B (UV-B) radiation on plant diseases," *Environmental Pollution*, vol. 88, no. 2, pp. 219–245, 1995.

[3] L. Willocquet, D. Colombet, M. Rougier, J. Fargues, and M. Clerjeau, "Effects of radiation, especially ultraviolet B, on conidial germination and mycelial growth of grape powdery mildew," *European Journal of Plant Pathology*, vol. 102, no. 5, pp. 441–449, 1996.

[4] X. C. Wu, W. X. Lin, Y. C. Guo, Y. Y. Liang, and F. Y. Chen, "Advance in research on the response of plants to the increased ultraviolet-B radiation," *Chinese Journal of Eco-Agriculture*, vol. 9, no. 3, pp. 52–55, 2001.

[5] A. H. Teramura and J. H. Sullivan, "Effects of UV-B radiation on photosynthesis and growth of terrestrial plants," *Photosynthesis Research*, vol. 39, no. 3, pp. 463–473, 1994.

[6] B. M. Greenberg, M. I. Wilson, K. E. Gerhardt, and K. E. Wilson, "Morphological and physiological responses of *Brassica napus* to ultraviolet-B radiation: photomodification of ribulose-1,5-bisphosphate carboxylase/oxygenase and potential acclimation processes," *Journal of Plant Physiology*, vol. 148, no. 1-2, pp. 78–85, 1996.

[7] M. A. K. Jansen, T. S. Babu, D. Heller, V. Gaba, A. K. Mattoo, and M. Edelman, "Ultraviolet-B effects on *Spirodela oligorrhiza*: induction of different protection mechanisms," *Plant Science*, vol. 115, no. 2, pp. 217–223, 1996.

[8] Å. Strid, W. S. Chow, and J. M. Anderson, "UV-B damage and protection at the molecular level in plants," *Photosynthesis Research*, vol. 39, no. 3, pp. 475–489, 1994.

[9] A. B. Britt, "DNA damage and repair in plants," *Annual Review of Plant Physiology and Plant Molecular Biology*, vol. 47, no. 1, pp. 75–100, 1996.

[10] J. Rozema, J. van de Staaij, L. O. Björn, and M. Caldwell, "UV-B as an environmental factor in plant life: stress and regulation," *Trends in Ecology and Evolution*, vol. 12, no. 1, pp. 22–28, 1997.

[11] J. Rotem, B. Wooding, and D. E. Aylor, "The role of solar radiation, especially ultraviolet, in the mortality of fungal spores," *Phytopathology*, vol. 75, no. 5, pp. 510–514, 1985.

[12] T. S. Gunasekera, N. D. Paul, and P. G. Ayres, "The effects of ultraviolet-U (UV-B: 290–320 nm) radiation on blister blight disease of tea (*Camellia sinensis*)," *Plant Pathology*, vol. 46, no. 2, pp. 179–185, 1997.

[13] L. B. Costa, D. E. N. Rangel, M. A. B. Morandi, and W. Bettiol, "Impact of UV-B radiation on *Clonostachys rosea* germination

and growth," *World Journal of Microbiology and Biotechnology*, vol. 28, no. 7, pp. 2497–2504, 2012.

[14] L. B. Costa, D. E. N. Rangel, M. A. B. Morandi, and W. Bettiol, "Effects of UV-B radiation on the antagonistic ability of *Clonostachys rosea* to *Botrytis cinerea* on strawberry leaves," *Biological Control*, vol. 65, no. 1, pp. 95–100, 2013.

[15] J. X. Jing, H. S. Shang, and Z. Q. Li, "The biological effects of ultraviolet ray radiadtion on wheat stripe rust (*Puccinia striiformis* West.)," *Acta Phytopathologica Sinica*, vol. 23, no. 4, pp. 299–304, 1993.

[16] H. S. Shang, J. X. Jing, and Z. Q. Li, "Mutations induced by ultraviolet radiation affecting virulence in *Puccinia striiformis*," *Acta Phytopathologica Sinica*, vol. 24, no. 4, pp. 347–351, 1994.

[17] L. L. Huang, X. L. Wang, Z. S. Kang, and J. Zhao, "Mutation of pathogenicity induced by ultrviolet radiation in *Puccinia striiformis* f. sp. *tritici* and RAPD analysis of mutants," *Mycosystema*, vol. 24, no. 3, pp. 400–406, 2005.

[18] X. L. Wang, F. Zhu, L. L. Huang, G. R. Wei, and Z. S. Kang, "Effects of ultraviolet radiation on pathogenicity mutation of *Puccinia striiformis* f. sp. *tritici*," *Journal of Nuclear Agricultural Sciences*, vol. 23, no. 3, pp. 375–379, 2009.

[19] X. L. Li, Z. H. Ma, L. L. Zhao, J. H. Li, and H. G. Wang, "Application of near infrared spectroscopy to qualitative identification and quantitative determination of *Puccinia striiformis* f. sp. *tritici* and *P. recondita* f. sp. *tritici*," *Spectroscopy and Spectral Analysis*, vol. 34, no. 3, pp. 643–647, 2014.

[20] Y. L. Yan, L. L. Zhao, D. H. Han, and S. M. Yang, *Basis and Application of Near Infrared Reflectance Spectroscopy*, China Light Industry Press, Beijing, China, 2005.

[21] G. E. Aiken, D. H. Pote, S. F. Tabler, and T. C. Tabler, "Application of near-infrared reflectance spectroscopy to estimate chemical constituents in broiler litter," *Communications in Soil Science and Plant Analysis*, vol. 36, no. 17-18, pp. 2529–2539, 2005.

[22] Q. Chen, J. Zhao, M. Liu, J. Cai, and J. Liu, "Determination of total polyphenols content in green tea using FT-NIR spectroscopy and different PLS algorithms," *Journal of Pharmaceutical and Biomedical Analysis*, vol. 46, no. 3, pp. 568–573, 2008.

[23] L. Feng, S. Chen, B. Feng, F. Liu, Y. He, and B. Lou, "Early detection of soybean pod anthracnose based on spectrum technology," *Transactions of the Chinese Society of Agricultural Engineering*, vol. 28, no. 1, pp. 139–144, 2012.

[24] B. Chen, S. K. Li, K. R. Wang et al., "Spectrum characteristics of cotton single leaf infected by verticillium wilt and estimation on severity level of disease," *Scientia Agricultura Sinica*, vol. 40, no. 12, pp. 2709–2715, 2007.

[25] D. Wu, L. Feng, C.-Q. Zhang, and Y. He, "Early detection of gray mold (Cinerea) on eggplant leaves based on Vis/near infrared spectra," *Journal of Infrared and Millimeter Waves*, vol. 26, no. 4, pp. 269–273, 2007.

[26] X. L. Li, Z. H. Ma, L. L. Zhao, J. H. Li, and H. G. Wang, "Early diagnosis of wheat stripe rust and wheat leaf rust using near infrared spectroscopy," *Spectroscopy and Spectral Analysis*, vol. 33, no. 10, pp. 2661–2665, 2013.

[27] C. Cortes and V. Vapnik, "Support-vector networks," *Machine Learning*, vol. 20, no. 3, pp. 273–297, 1995.

[28] C. C. Chang and C. J. Lin, "LIBSVM: a Library for support vector machines," *ACM Transactions on Intelligent Systems and Technology*, vol. 2, no. 3, article 27, 2011.